Optics & Laser Technology 151 (2022) 108077

Contents lists available at ScienceDirect

Optics and Laser Technology

journal homepage: www.elsevier.com/locate/optlastec

Megahertz ultrasonic source induced by femtosecond laser irradiation of graphene foam

Tingyuan Wang [a], Kai Zhao [b], Zhen Ge [b], Yongsheng Chen [b], Lie Lin [a,c], Nan Zhang [a,*], Weiwei Liu [a]

[a] Institute of Modern Optics, Nankai University, Tianjin Key Laboratory of Micro-scale Optical Information Science and Technology, Tianjin 300350, China
[b] Key Laboratory for Functional Polymer Materials and The Centre for Nanoscale Science and Technology, Institute of Polymer Chemistry, Synergetic Innovation Center of Chemical Science and Engineering (Tianjin), College of Chemistry, Nankai University, Tianjin 300071, China
[c] Tianjin Key Laboratory of Optoelectronic Sensor and Sensing Network Technology, Tianjin 300350, China

ARTICLE INFO

Keywords:
Megahertz ultrasonic source
Femtosecond laser
Graphene foam
Photo-thermo-acoustic effect

ABSTRACT

The performance of a photo-thermo-acoustic (PTA) ultrasonic source can be significantly improved by utilizing graphene-based materials. Graphene is an excellent PTA material owing to its wide electromagnetic absorption spectrum, low heat capacity per unit area, and high thermal conductivity. In this study, a broadband graphene-foam-based PTA ultrasonic source covering the frequency range of 50 kHz to 1.8 MHz was excited by a near-infrared femtosecond laser beam. The lower and upper frequency limits of the acoustic wave that can be detected in the experiments were determined by the responsivity of the microphone and the attenuation of the acoustic wave in air, respectively. The experimental results show that the sound pressure of this ultrasonic source was independent of the laser polarization and incident angle. The peak-to-peak magnitude of the ultrasonic wave was proportional to laser energy when the single-pulse energy of the femtosecond laser varied from 0.4 to 1.0 mJ. Therefore, the sound intensity of the ultrasonic source could be easily controlled by modulating the laser energy. The experimental results also show that the ultrasonic wave emitted from the graphene foam had a dipole-like acoustic pressure distribution, and its principal emission direction was normal to the sample surface, regardless of the laser incidence angle. This characteristic may benefit future applications in directed message transfer/acquisition and nondestructive testing/imaging.

1. Introduction

Megahertz (MHz) ultrasonic sources have been widely used in nondestructive testing [1–3], medical treatment [4], and high-resolution biomedical imaging [5,6]. Limited by its electromechanical resonance principle, the bandwidth of the MHz piezoelectric ultrasonic source is only several kilohertz [7]. In contrast, by utilising the photo-thermo-acoustic (PTA) effect [8,9], one can produce MHz/gigahertz (GHz) ultrasonic sources with a flat and wide acoustic spectrum [10,11], the bandwidths of which can reach MHz or even GHz [12–14]. An ultrabroadband ultrasonic source can achieve a much higher heating efficiency in multiple-frequency biotissue cutting [15] and better temporal resolution in testing and imaging [16]. Furthermore, compared with the MHz piezoelectric ultrasonic source, the PTA ultrasonic source can resist to the electromagnetic interference and achieve remote control without any type of physical connection.

Although the PTA effect has been known for nearly 140 years [17], the development of the PTA ultrasonic source was hindered by the low photoacoustic conversion efficiency of conventional materials until the emergence of graphene and graphene-based materials. The Dirac-type band structure [18], low heat capacity per unit area (HCPUA) [19,20], and high thermal conductivity [19] of graphene-based materials make them ideal PTA materials with high photoacoustic conversion efficiency [21–24]. A band structure of this type leads to a broad electromagnetic absorption band from terahertz (THz) to ultraviolet (UV) wavelengths [25], whereas the low HCPUA facilitates heating to a high temperature. Finally, the high thermal conductivity results in a higher sound pressure during the thermoacoustic (TA) conversion process [21,26]. Compared

Abbreviations: PTA, photo-thermo-acoustic; HCPUA, low heat capacity per unit area; MHz, Megahertz; GHz, megahertz/gigahertz; THz, terahertz; UV, ultraviolet; HWP, half-wave plate; FWHM, full width at half maxima; RSD, relative standard deviation; PT, photo-thermal; TA, thermo-acoustic.

* Corresponding author at: Institute of Modern Optics, No. 38 Tongyan Road, Jinnan District, Nankai University, Tianjin 300350, China.
E-mail address: zhangn@nankai.edu.cn (N. Zhang).

https://doi.org/10.1016/j.optlastec.2022.108077
Received 21 August 2021; Received in revised form 10 March 2022; Accepted 14 March 2022
Available online 19 March 2022

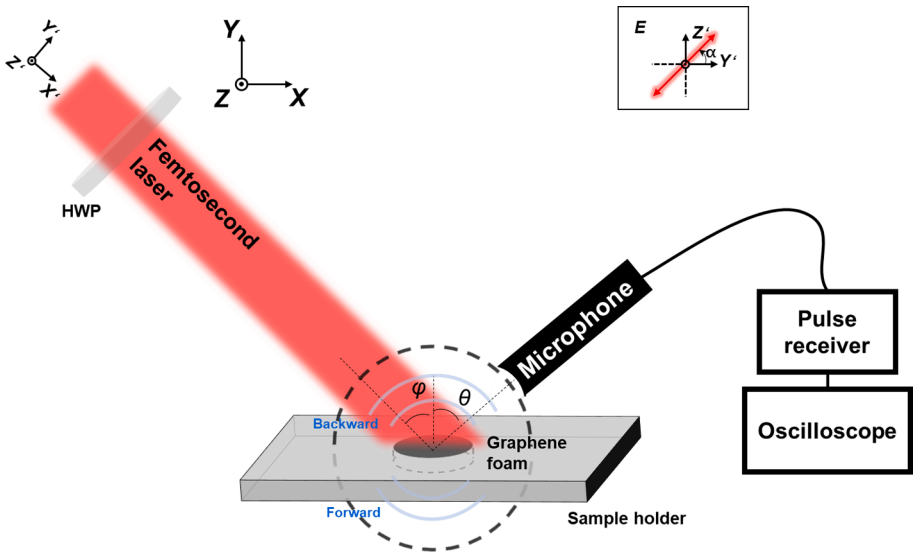

Fig. 1. Schematic diagram of the experimental setup for ultrasonic wave generation by femtosecond laser irradiation of graphene foam: HWP, half-wave plate (in this figure, the *z*- and *z*'-axes are identical).

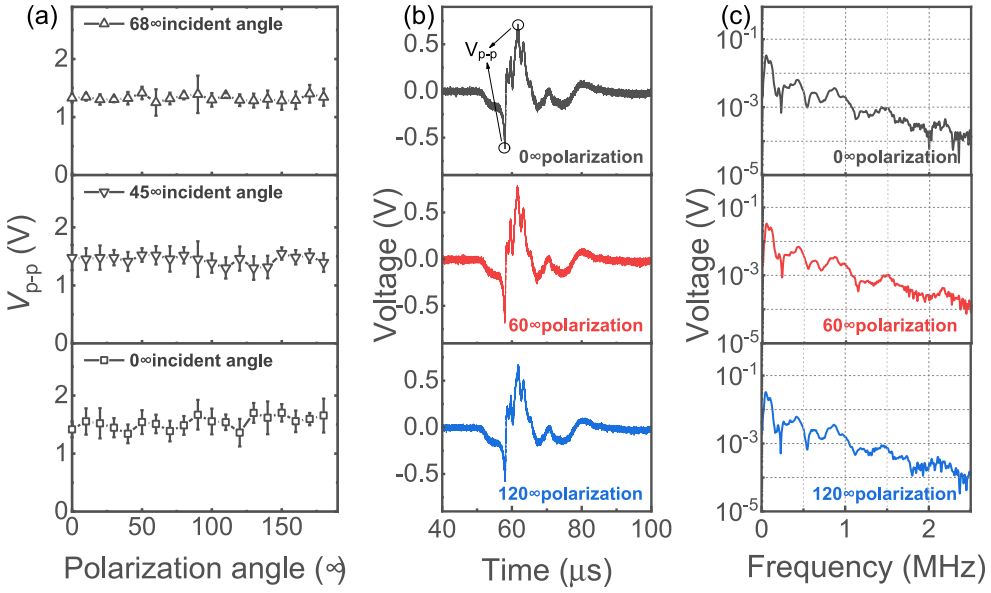

Fig. 2. (a) Dependence of the peak-to-peak magnitude of ultrasonic wave emitted from the top sample surface (see Fig. 1) on the polarization direction of the femtosecond laser: the typical time domain waveforms of the ultrasonic waves in the time range of 40–100 μs are presented in (b), and the corresponding Fourier transforms are presented in (c).

with graphene sheets, graphene foam has a higher photoacoustic conversion efficiency because no substrate is required for graphene foam and heat leakage to the substrate is avoided.

In this study, a MHz PTA ultrasonic source was produced by irradiating graphene foam with near-infrared femtosecond laser pulses. The effects of laser polarization and energy on the generated ultrasonic wave and the directivity of the ultrasonic emission were investigated experimentally. The experimental results reveal that the peak-to-peak amplitude of the ultrasonic wave was proportional to the laser energy and independent of the polarization and incident angle of the femtosecond laser. Therefore, the sound energy could be easily modulated by adjusting the input laser energy. The experiments also show that the ultrasonic wave emission had a dipole-like acoustic pressure distribution, and the preferential emission direction was normal to the sample surface, regardless of the incident angle. In addition, under the striking of femtosecond laser, the ultrasonic wave was emitted from both sides of the graphene foam sample; the forward and backward acoustic emissions had identical directivities and dependences on laser parameters. These properties make the ultrasonic wave generated from graphene foam potentially applicable in directed message transfer and imaging.

2. Materials and methods

A schematic diagram of the experimental setup used to generate the MHz ultrasonic wave is shown in Fig. 1. Laser pulses of 35 fs, 800 nm, and 500 Hz with a single pulse energy of 1.0 mJ are produced by a commercial Ti: sapphire chirped pulse amplification system (Legend Elite, Coherent, Inc.). The linearly polarized femtosecond laser beam has a 10-mm beam diameter ($1/e^2$ spot size). The output laser energy can be continuously adjusted by the combination of a half-wave plate and the compressor grating, both of which are located inside the amplification system. Another half-wave plate (see Fig. 1) outside the amplification

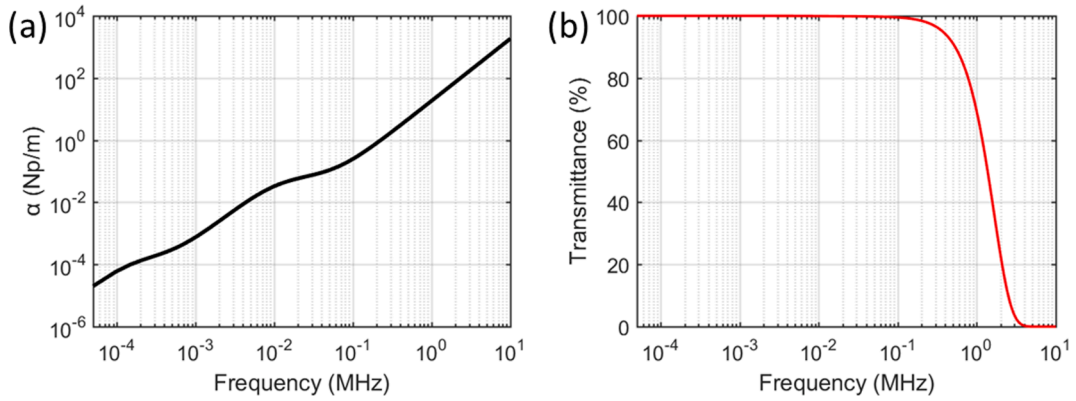

Fig. 3. (a) Acoustic wave attenuation coefficient in 1 atm, 20 °C air with 20% relative humidity and (b) calculated transmittance of the acoustic wave after propagating 20 mm from the graphene foam surface to the microphone.

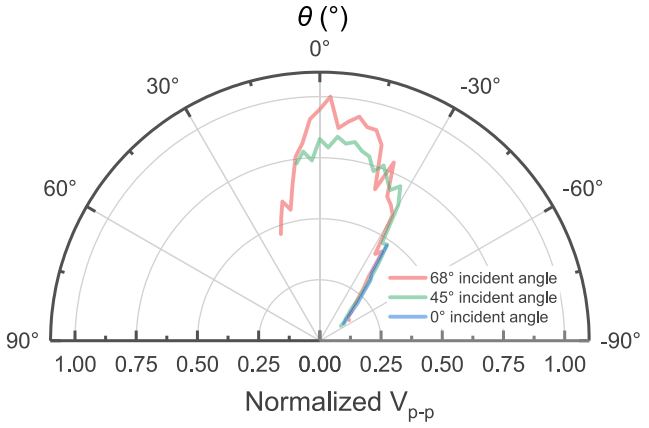

Fig. 4. Emission directivity of the backward ultrasonic wave produced by femtosecond laser irradiation of graphene foam: the incident angles of the femtosecond laser are 68° (red line), 45° (green line), and 0° (blue line), and the pulse energy of the femtosecond laser is 1.0 mJ. (For interpretation of the references to colour in this figure legend, the reader is referred to the web version of this article.)

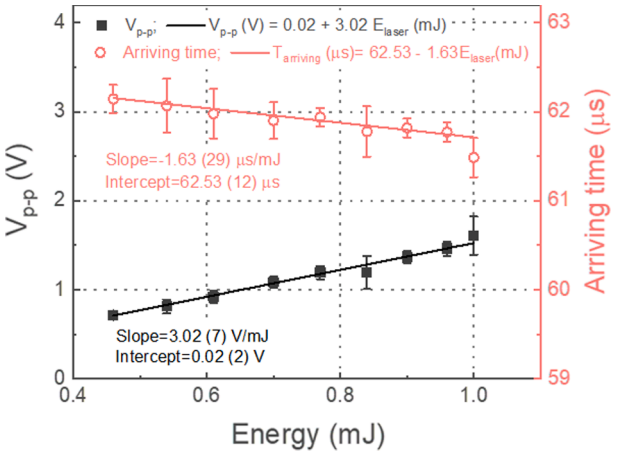

Fig. 5. Femtosecond laser pulse energy effect on the backward ultrasonic wave: the pump laser irradiates the graphene foam at an incident angle of 68°, and the detection angle of the microphone is − 35°; the square and circle data points respectively indicate the peak-to-peak voltage and the arriving time of the ultrasonic pulse; some error bars are so small that they are covered by the data points. The linear fittings (red and black solid lines) of the square and circle data points are both weighted by the error bars.

system is employed to rotate the laser polarization. Angle α indicates the orientation of the laser polarization, which is defined as the angle between the polarization and the y'-axis (see the inset in Fig. 1). Here, $\alpha > 0°$ and $\alpha < 0°$, respectively, indicate that the polarization rotates anticlockwise and clockwise relative to the y'-axis. The femtosecond laser beam irradiates the graphene foam at an incident angle φ. The graphene foam sample has a cylindrical shape with a diameter of 10 mm and thickness of 2 mm. A microphone (V306, Olympus, Ltd.) combined with an ultrasonic pulse receiver (5072PR, Olympus, Ltd.) is used to detect the generated ultrasonic wave, which is displayed on an oscilloscope (DPO3034, Tektronix, Inc.). The microphone is mounted on a rotatory stage and can be moved along the dashed circle with a radius of 20 mm, as shown in Fig. 1. The location of the microphone is denoted by angle θ.

During the experiments, a femtosecond laser with different incident angles of $\varphi = 68°$, 45°, and 0° is employed to irradiate the graphene foam. Ultrasonic waves are emitted from the top and bottom surfaces of the graphene foam, as indicated by the blue arcs in Fig. 1. Because the full width at half maximum diameter of the laser beam is equal to the diameter of the graphene foam sample, the sound emission areas are constant for different incident angles, which are all equal to the sample surface area. The laser pulse energy indicated hereinafter is the effective laser pulse energy, which is obtained by measuring the laser energy transmitted through the sample holder after removing the graphene foam from the holder.

Graphene is an excellent 2D TA material. First, graphene has an extremely low HCPUA of 5.8×10^{-4} J m^{-2} K^{-1} (HCPUA = $d\rho C_p$, where d, ρ, and C_p are the thickness, density, and constant-pressure specific heat of graphene, respectively) [26] because it is the thinnest known material (0.34 nm). The HCPUA is inversely proportional to the acoustic pressure [27], so graphene is one of the best TA materials, generating a very high acoustic pressure [20]. Furthermore, the high thermal conductivity (5300 W m^{-1} K^{-1}) of graphene benefits the production of acoustic waves owing to the rapid heat transfer to the ambient material [21,26]. The graphene foam sample used in the experiments is a 3D crosslinked monolithic graphene material with an ultrahigh void ratio of as much as 99.9% and low density of 1 mg/cm^3. It can be regarded as a macro-aggregation of many electronically isolated and structurally suspended graphene sheets. There is no strong chemical bond structure between adjacent graphene sheets in the sample. Therefore, the graphene foam retains the properties of graphene, including the Dirac-type band structure and photoelectric and TA properties. Furthermore, the heat leakage of the graphene foam to the substrate is much smaller than that of few-layer graphene, which can further improve the performance of TA devices. The detailed synthesis processes and parameters of the graphene foam are described elsewhere [28].

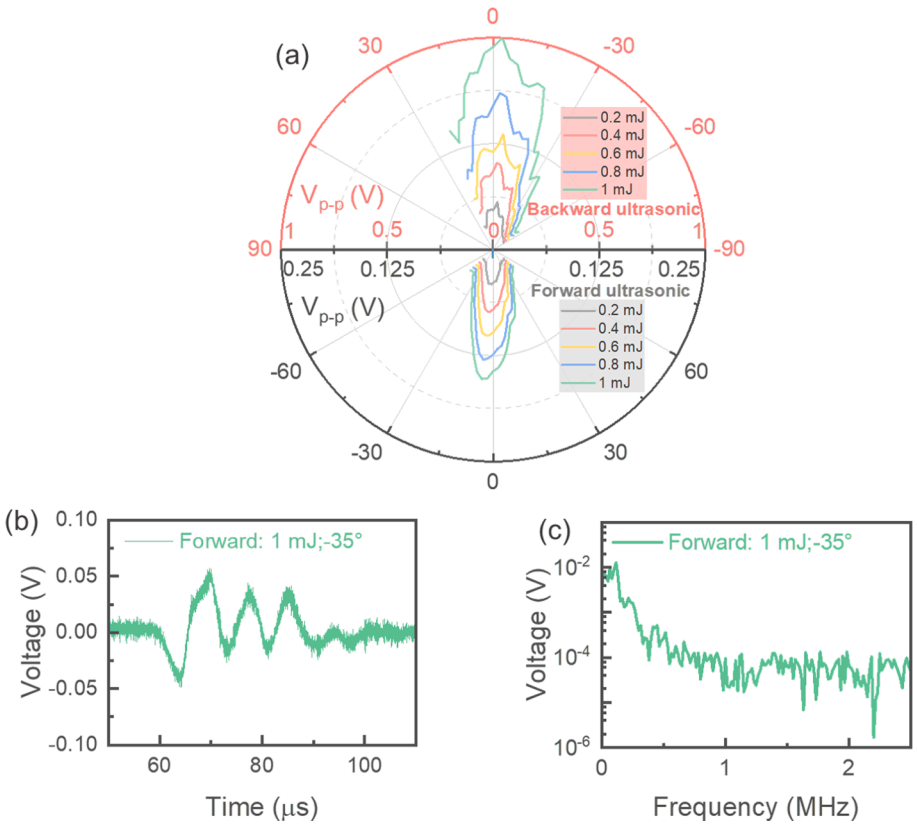

Fig. 6. (a) Emission directivity of the forward and backward ultrasonic waves under the irradiation of femtosecond laser with different pulse energies, where the pump femtosecond laser irradiates the graphene foam at an incident angle of 68°, (b) and (c) the time domain waveforms and corresponding spectrum, respectively, of the forward ultrasonic waves generated by 1.0-mJ femtosecond laser pulse, where the detection angle is −35°, and (c) spectrum obtained by Fourier transforming the signal in (b) in a time window of 50–110 μs.

3. Results and discussion

The voltage V shown in Fig. 2 represents the sound pressure P through the voltage-to-pressure responsivity β which is a frequency-dependent coefficient describing the piezoelectric response of the microphone [29]. Therefore, the peak-to-peak voltage $V_{p\text{-}p}$ of the ultrasonic pulse in Fig. 2(a) represents the amplitude of the acoustic pulse sound pressure. As Fig. 2(a) shows, a femtosecond laser with a single pulse energy of 1.0 mJ irradiates the graphene foam at incident angles of 68°, 45°, and 0°. The detection angle θ (see Fig. 1) is − 35° for all cases. The average relative standard deviation of all data points in Fig. 2(a) is approximately 8%, which implies that the intensity of the backward ultrasonic wave (i.e., the one emitted from the top sample surface in Fig. 1) is independent of the polarization of the femtosecond laser. Polarization independent characteristics can also be seen from the time domain and frequency domain waveforms of the backward ultrasonic waves, which are presented in Fig. 2(b) and (c), respectively. This polarization independent characteristic may originate from the polarization independent absorbance of graphene. The absorbance of graphene in the infrared-to-visible range is approximately a constant that is independent of laser polarization [30,31]. In addition, Fig. 2(a) indicates that changing the incident angle of the laser does not affect the backward ultrasonic wave.

As shown in Fig. 2(c), the ultrasonic pulse emitted from the graphene foam covers the frequency range from 50 kHz to 1.8 MHz. The low-frequency limit is determined by the frequency response limit of the piezoelectric microphone used in the experiments [29,32]. The upper frequency limit is mainly determined by the attenuation of ultrasonic waves in air. Such a broadband ultrasonic pulse generated by graphene foam is more suitable for ultrasound therapy than narrowband/single-frequency ultrasonic waves because multifrequency ultrasonic waves are more efficient in heating the tissue and inducing a larger treating volume [15].

The upper frequency limit of the ultrasonic waves detected in the experiments is mainly determined by the PTA mechanism and attenuation of acoustic waves in air. In the photothermal (PT) conversion process [24], first, the femtosecond laser is absorbed by the electrons of the graphene foam and excites the electrons to the conduction band in the femtosecond timescale [33]. Second, the electron–phonon scattering causes the generation of hot optical phonons on a picosecond timescale [33,34]. Third, the temperatures of the electrons and phonons decrease owing to the emission of acoustic phonons out of the laser deposition volume on a nanosecond timescale [35]. In the TA conversion stage [21,24], the acoustic phonons diffuse and heat the air layer adjacent to the sample surface, inducing quick expansion of the adjacent air layer and producing an acoustic pulse. This acoustic pulse has a pulse duration several times longer than the heating time of the air layer [36]. Therefore, the upper frequency limit of the ultrasonic wave near the sample surface is mainly determined by the timescale of the heating process of the air layer.

The acoustic pressure after propagating a distance z is $P(z) = P_0 e^{-\alpha z}$ [37], where P_0 is the acoustic pressure at the graphene foam surface, and α is the attenuation coefficient, which can be obtained from previous research [37–40]. Fig. 3(a) and (b) show, respectively, the frequency-dependent attenuation coefficient of the acoustic wave in air and the calculated acoustic transmittance at the microphone after the ultrasonic wave propagated 20 mm from the graphene foam surface. In Fig. 3(a), the unit of the acoustic attenuation coefficient α is N_p/m and 1 N_p/m indicates that the pressure of the acoustic wave will be attenuated to 1/e of the initial pressure after propagating 1 m in the medium. The transmittance is approximately 99% at 100 kHz and 45% at 1.5 MHz, but only 20% and 10% at 2 and 2.5 MHz, respectively. The peak responsivity of the microphone used in the experiments appears at 2.3 MHz. Therefore, combining the calculations in Fig. 3(c) and the experimental results in Fig. 2(c) reveals that the upper detection limit of 1.8 MHz is mainly caused by the attenuation of the ultrasonic waves in air.

Fig. 4 presents the measured emission directivity of the backward ultrasonic wave produced by femtosecond laser irradiation of the

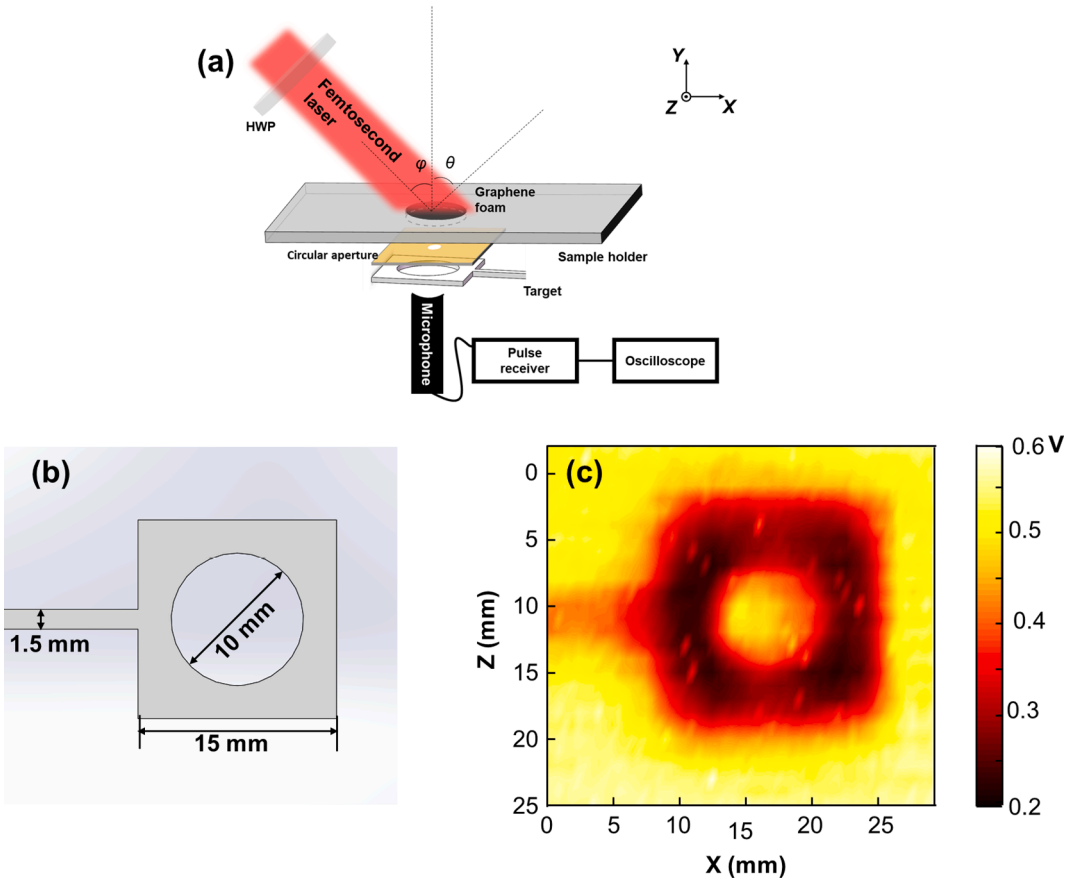

Fig. 7. Acoustic imaging using the forward ultrasonic wave generated by the graphene foam: (a) schematic diagram of the graphene foam ultrasonic imaging, with the femtosecond laser striking on the graphene foam at an incident angle of 68° and a femtosecond laser single-pulse energy of 1.0 mJ, (b) schematic diagram of the polylactic acid target with a thickness of 0.8 mm, and (c) ultrasonic image of the target.

graphene foam. $V_{p\text{-}p}$ is obtained from the measured temporal profile of the acoustic pulse emitted from the graphene foam (see Fig. 2(b)). The normalized $V_{p\text{-}p}$ in Fig. 4 is calculated by dividing the measured $V_{p\text{-}p}$ by the maximal $V_{p\text{-}p}$. The maximal $V_{p\text{-}p}$ appears near the normal of the graphene foam surface during the irradiation of femtosecond laser with an incident angle of 68°. The detection angle range is limited by the geometrical dimensions of the microphone and the relative position between the microphone and the femtosecond laser beam. For example, in the case of an incident angle of 68°, the ultrasonic wave at $\theta > 20°$ cannot be measured because the laser beam is blocked by the microphone. Comparing the ultrasonic emission directivities at these three incident angles reveals that, in the measurable angle range, the emission directivity of the ultrasonic wave is independent of the incident angle of the femtosecond laser. For laser beams with incident angles of 45° and 68°, the ultrasonic wave emitted from the top surface of the graphene foam exhibits a dipole-like directivity whose preferential direction is normal to the sample surface. The emission directivity of the ultrasonic waves produced from graphene foam might benefit applications in directed information transfer/acquisition and remote nondestructive testing/imaging.

Fig. 5 shows the effect of femtosecond laser energy on the ultrasonic wave pressure and arrival time at the microphone. Because a higher laser energy causes damage to the graphene foam, the effective laser energy striking the graphene foam sample is no>1.0 mJ. For the experimental results shown in Fig. 5, the incident angle of the femtosecond laser is 68°, and the detection angle of the microphone is − 35°. The corresponding results for the other incident angles and detection angles are similar to those in Fig. 5 and are not presented here. Fig. 5 shows that a linear relationship exists between the peak-to-peak voltage (i.e., the amplitude of the acoustic pressure) and the single-pulse energy of the femtosecond laser. In addition, Fig. 5 shows the dependence of the arrival time of the ultrasonic pulse at the microphone on femtosecond laser energy. Although the distance between the microphone and graphene foam sample remains constant, the ultrasonic arrival time decreases as the femtosecond laser energy increases. This phenomenon may originate from the PTA acoustic wave generation process. Because the PT stage completes within several nanoseconds based on the above analyses and the variation of the arrival time in Fig. 5 can be as much as 0.5 μs, the variation in the arrival time must come from the TA stage.

According to Fourier's heat conduction law [41], in the TA stage, the heat flow Q between the hot graphene foam and the cool adjacent air layer is proportional to the temperature difference ΔT. The temperature difference can be calculated by $\Delta T = \eta_{PT}\alpha_o E/C_{GF}$, where η_{PT} , α_o, E, and C_{GF} are the PT conversion efficiency, optical absorption coefficient, pulse energy of the femtosecond laser, and heat capacity of the graphene foam sample with unit thickness, respectively. Therefore, Q is proportional to E, i.e., $Q = \gamma E$, and γ is a proportional coefficient. It is considered that when the air layer adjacent to the graphene foam is heated to a certain temperature T_{th} with a sufficiently large pressure, the emission of the acoustic wave begins. Consequently, the emitting time t_e of the acoustic wave can be estimated using the equation $\gamma E t_e = C_{air}T_{th}$, where C_{air} is the heat capacity of the adjacent air layer. Therefore, the relationship between the emission time of the acoustic wave and the laser energy can be expressed as $t_e = C_{air}T_{th}/(\gamma E)$. After the Taylor expansion around E_0 (E_0 is an arbitrary value from 0.4 to 1.0 mJ) is applied, and ignoring high-order terms, it is found that the emitting time of the acoustic wave decreases with the increase in the laser pulse energy, which obeys the relation $t_e = C_{air}T_{th}(2E_0 - E)/(\gamma E_0^2)$. This explains

the dependence of the arrival time of the acoustic wave on the laser pulse energy, as shown in Fig. 5.

Fig. 6(a) shows that the emission directivities of the forward and backward ultrasonic waves exhibit a dipole-like acoustic pressure distribution with a preferential direction perpendicular to the graphene foam surface. Fig. 6(a) also reveals that, for the forward and backward acoustic emissions, the amplitude of the ultrasonic wave increases proportionally as the laser pulse energy increases. Furthermore, the peak-to-peak magnitude of the forward ultrasonic wave is only 15% that of the backward one when the femtosecond laser pulse energy is 1.0 mJ. The following physical scenario may help to understand why the forward ultrasonic wave is weaker. The deposited laser energy per unit sample thickness gradually decreases as the depth increases and is highest on the top surface of the graphene foam. Therefore, the acoustic pressure of the ultrasonic wave generated at a specific depth of the graphene foam also decreases as the depth increases. Considering the attenuation during the acoustic wave propagation inside the graphene foam, one can infer that the forward ultrasonic wave is much weaker than the backward one. Meanwhile, the forward ultrasonic wave has a lower high-frequency component than the backward one, as shown in Figs. 2 and 6(c). The high-frequency component loss may be caused by the propagation of the forward ultrasonic pulse through the porous graphene foam.

As a practical application of the ultrasonic wave generated by the graphene foam, an acoustic imaging experiment was performed, and the results are shown in Fig. 7. To enhance the imaging resolution, a small circular aperture with a diameter of 3 mm was placed before the imaging target to reduce the acoustic beam diameter. A microphone was placed perpendicular to the target to collect the transmitted acoustic wave. The microphone and target were 20 and 14 mm from the top surface of the graphene foam, respectively. Fig. 7(b) is a schematic diagram of the target, which moved along the *X*- and *Z*-directions with a step of 0.5 mm during the imaging process. The measured ultrasonic imaging results are shown in Fig. 7(c). Because the size of the ultrasonic beam in the near field is determined by the diameter of the circular aperture rather than the diffraction limit, the imaging resolution can be improved by simply reducing the aperture diameter. At present, the sensitivity of the microphone hinders further reduction of the aperture diameter and improvement of the imaging resolution.

4. Conclusions

MHz ultrasonic waves were produced by femtosecond laser irradiation of graphene foam, and the physical origin and critical limiting factors of the ultrasonic bandwidth were investigated. The bandwidth of the ultrasonic wave generated by graphene foam is obviously larger than those generated by piezoelectric transducers and can achieve higher heating efficiency in multiple-frequency biotissue cutting [15]. The ultrasonic pulse generated from the graphene foam has a dipole-like emission directivity, and its acoustic pressure is independent of the polarization and incident angle of the femtosecond laser. Furthermore, the amplitude of the ultrasonic wave is proportional to the laser pulse energy, which is convenient for adjusting the ultrasonic wave intensity in practical applications.

CRediT authorship contribution statement

Tingyuan Wang: Software, Validation, Formal analysis, Writing – original draft, Writing – review & editing. **Kai Zhao:** Resources, Writing – review & editing. **Zhen Ge:** Resources, Writing – review & editing. **Yongsheng Chen:** Resources, Writing – review & editing. **Lie Lin:** Writing – review & editing. **Nan Zhang:** Conceptualization, Methodology, Software, Validation, Formal analysis, Resources, Writing – original draft, Writing – review & editing, Supervision, Project administration, Funding acquisition. **Weiwei Liu:** Writing – review & editing, Funding acquisition.

Declaration of Competing Interest

The authors declare that they have no known competing financial interests or personal relationships that could have appeared to influence the work reported in this paper.

Acknowledgements

This work is supported by National Key Research and Development Program of China (2018YFB0504400), National Natural Science Foundation of China (12061131010, 12074198) and Russian Science Foundation (RSF) (21-49-00023).

References

[1] C.B. Scruby, L.E. Drain, Laser Ultrasonics, Routledge (1990), https://doi.org/10.1201/9780203749098.
[2] V.V. Kozhushko, P. Hess, Laser-induced focused ultrasound for nondestructive testing and evaluation, J. Appl. Phys. 103 (12) (2008) 124902.
[3] I. Pelivanov, T. Buma, J. Xia, C. Wei, M. O'Donnell, NDT of fiber-reinforced composites with a new fiber-optic pump–probe laser-ultrasound system, Photoacoustics. 2 (2014) 63–74, https://doi.org/10.1016/j.pacs.2014.01.001.
[4] T.J. Dubinsky, C. Cuevas, M.K. Dighe, O. Kolokythas, J.H. Hwang, High-Intensity Focused Ultrasound: Current Potential and Oncologic Applications, Am. J. Roentgenol. 190 (2008) 191–199, https://doi.org/10.2214/AJR.07.2671.
[5] J. Kim, S. Park, Y. Jung, S. Chang, J. Park, Y. Zhang, J.F. Lovell, C. Kim, Programmable Real-time Clinical Photoacoustic and Ultrasound Imaging System, Sci. Rep. 6 (2016) 35137, https://doi.org/10.1038/srep35137.
[6] C. Moore, J.V. Jokerst, Strategies for Image-Guided Therapy, Surgery, and Drug Delivery Using Photoacoustic Imaging, Theranostics. 9 (2019) 1550–1571, https://doi.org/10.7150/thno.32362.
[7] J. Borwick, Loudspeaker and Headphone Handbook (2012).
[8] A. Rosencwaig, A. Gersho, Theory of the photoacoustic effect with solids, J. Appl. Phys. 47 (1976) 64–69, https://doi.org/10.1063/1.322296.
[9] S. Manohar, D. Razansky, Photoacoustics: a historical review, Adv. Opt. Photonics. 8 (2016) 586, https://doi.org/10.1364/AOP.8.000586.
[10] D.A. Hutchins, Mechanisms of Pulsed Photoacoustic Generation, Can. J. Phys. 64 (1985) 1247–1264, https://doi.org/10.1139/p86-217.
[11] M. Daschewski, R. Boehm, J. Prager, M. Kreutzbruck, A. Harrer, Physics of thermo-acoustic sound generation, J. Appl. Phys. 114 (11) (2013), https://doi.org/10.1063/1.4821121.
[12] T. Dehoux, M.A. Ghanem, O.F. Zouani, J.-M. Rampnoux, Y. Guillet, S. Dilhaire, M.-C. Durrieu, B. Audoin, All-optical broadband ultrasonography of single cells, Sci. Rep. 5 (2015) 8650, https://doi.org/10.1038/srep08650.
[13] S. Hwan Lee, M.-a. Park, J.J. Yoh, H. Song, E. Yun Jang, Y. Hyup Kim, S. Kang, Y. Seop Yoon, Reduced graphene oxide coated thin aluminum film as an optoacoustic transmitter for high pressure and high frequency ultrasound generation, Appl. Phys. Lett. 101 (24) (2012), https://doi.org/10.1063/1.4772498.
[14] W. Xiong, R.S. Witte, H. Xin, Thermoacoustic and photoacoustic characterizations of few-layer graphene by pulsed excitations, Appl. Phys. Lett. 108 (2016), 143104, https://doi.org/10.1063/1.4945661.
[15] G. Sijia, J. Xiaoning, L. Weili, Tissue ablation using multi-frequency focused ultrasound, in: 2011 IEEE Int. Ultrason. Symp., IEEE, 2011: pp. 2177–2180. doi:10.1109/ULTSYM.2011.0540.
[16] R.H. Silverman, E. Vinarsky, S.M. Woods, F.L. Lizzi, D.J. Coleman, The effect of transducer bandwidth on ultrasonic image characteristics, Retina. 15 (1995) 37–42, https://doi.org/10.1097/00006982-199515010-00008.
[17] A.G. Bell, On the production and reproduction of sound by light, Am. J. Sci. 29 (1880) 305–324, https://doi.org/10.2475/ajs.s3-20.118.305.
[18] A.K. Geim, K.S. Novoselov, The rise of graphene, in: Nanosci. Technol., Co-Published with Macmillan Publishers Ltd, UK, 2009: pp. 11–19. doi:10.1142/9789814287005_0002.
[19] E. Pop, V. Varshney, A.K. Roy, Thermal properties of graphene: Fundamentals and applications, MRS Bull. 37 (2012) 1273–1281, https://doi.org/10.1557/mrs.2012.203.
[20] Y. Qiao, G. Gou, F. Wu, J. Jian, X. Li, T. Hirtz, Y. Zhao, Y. Zhi, F. Wang, H. Tian, Y. Yang, T.-L. Ren, Graphene-Based Thermoacoustic Sound Source, ACS Nano. 14 (2020) 3779–3804, https://doi.org/10.1021/acsnano.9b10020.
[21] F. Giorgianni, C. Vicario, M. Shalaby, L.D. Tenuzzo, A. Marcelli, T. Zhang, K. Zhao, Y. Chen, C. Hauri, S. Lupi, CSY High-Efficiency and Low Distortion Photoacoustic Effect in 3D Graphene Sponge, Adv. Funct. Mater. 28 (2018) 1702652, https://doi.org/10.1002/adfm.201702652.
[22] N. Yang, S. Li, C. Li, X. Fan, The Photoacoustic Effect of Multilayered Graphene Films, IOP Conf. Ser. Mater. Sci. Eng. 531 (1) (2019) 012085, https://doi.org/10.1088/1757-899X/531/1/012085.
[23] F. De Nicola, L.D. Tenuzzo, I. Viola, R. Zhang, H. Zhu, A. Marcelli, S. Lupi, Ultimate Photo-Thermo-Acoustic Efficiency of Graphene Aerogels, Sci. Rep. 9 (2019) 13386, https://doi.org/10.1038/s41598-019-50082-7.
[24] Y. Tian, H. Tian, Y.L. Wu, L.L. Zhu, L.Q. Tao, W. Zhang, Y. Shu, D. Xie, Y. Yang, Z. Y. Wei, X.H. Lu, T. Ren, C. Shih, J. Zhao, Coherent Generation of Photo-Thermo-

Acoustic Wave from Graphene Sheets, Sci. Rep. 5 (2015) 10582, https://doi.org/10.1038/srep10582.
[25] K.F. Mak, L. Ju, F. Wang, T.F. Heinz, Optical spectroscopy of graphene: From the far infrared to the ultraviolet, Solid State Commun. 152 (2012) 1341–1349, https://doi.org/10.1016/j.ssc.2012.04.064.
[26] J.W. Suk, K. Kirk, Y. Hao, N.A. Hall, R.S. Ruoff, Thermoacoustic sound generation from monolayer graphene for transparent and flexible sound sources, Adv. Mater. 24 (2012) 6342–6347, https://doi.org/10.1002/adma.201201782.
[27] H. Hu, T. Zhu, J. Xu, Model for thermoacoustic emission from solids, Appl. Phys. Lett. 96 (21) (2010), https://doi.org/10.1063/1.3435429.
[28] Y. Wu, N. Yi, L. Huang, T. Zhang, S. Fang, H. Chang, N. Li, J. Oh, J.A. Lee, M. Kozlov, A.C. Chipara, H. Terrones, P. Xiao, G. Long, Y. Huang, F. Zhang, L. Zhang, X. Lepró, C. Haines, M.D. Lima, N.P. Lopez, L.P. Rajukumar, A.L. Elias, S. Feng, S.J. Kim, N.T. Narayanan, P.M. Ajayan, M. Terrones, A. Aliev, P. Chu, Z. Zhang, R.H. Baughman, Y. Chen, Three-dimensionally bonded spongy graphene material with super compressive elasticity and near-zero Poisson's ratio, Nat. Commun. 6 (2015) 6141, https://doi.org/10.1038/ncomms7141.
[29] K. Ono, Frequency dependence of receiving sensitivity of ultrasonic transducers and acoustic emission sensors, Sensors. 18 (2018) 3861, https://doi.org/10.3390/s18113861.
[30] K.F. Mak, M.Y. Sfeir, Y. Wu, C.H. Lui, J.A. Misewich, T.F. Heinz, Measurement of the Optical Conductivity of Graphene, Phys. Rev. Lett. 101 (2008), https://doi.org/10.1103/PhysRevLett.101.196405.
[31] R.R. Nair, P. Blake, A.N. Grigorenko, K.S. Novoselov, T.J. Booth, T. Stauber, N.M. R. Peres, A.K. Geim, Fine structure constant defines visual transparency of graphene, Science. 320 (2008), https://doi.org/10.1126/science.1156965.
[32] M. Toa, A. Whitehead, Ultrasonic Sensing Basics, Texas Instruments. (2020) 1–15. https://www.ti.com/lit/an/slaa907c/slaa907c.pdf?ts=1626327189202&ref_url=https%253A%252F%252Fcn.bing.com%252F.
[33] J.M. Dawlaty, S. Shivaraman, M. Chandrashekhar, F. Rana, M.G. Spencer, Measurement of ultrafast carrier dynamics in epitaxial graphene, Appl. Phys. Lett. 92 (4) (2008), https://doi.org/10.1063/1.2837539.
[34] J.C.W. Song, L.S. Levitov, Energy flows in graphene: Hot carrier dynamics and cooling, J. Phys. Condens. Matter. 27 (2015) 24–27, https://doi.org/10.1088/0953-8984/27/16/164201.
[35] W.K. Tse, S. Das Sarma, Energy relaxation of hot Dirac fermions in graphene, Phys. Rev. B. 79 (2009), 235406, https://doi.org/10.1103/PhysRevB.79.235406.
[36] Y. Huang, H.H. Bau, Thermoacoustic waves in a semi-infinite medium, Int. J. Heat Mass Transf. 38 (1995) 1329–1345, https://doi.org/10.1016/0017-9310(94)00271-V.
[37] K. Nakamura, Ultrasonic transducers, Woodhead Publishing Limited (2012), https://doi.org/10.1533/9780857096302.
[38] L.J. Bond, C. Chiang, C.M. Fortunko, Absorption of ultrasonic waves in air at high frequencies (10–20 MHz), J. Acoust. Soc. Am. 92 (1992) 2006–2015, https://doi.org/10.1121/1.405251.
[39] H.E. Bass, L.C. Sutherland, A.J. Zuckerwar, Atmospheric absorption of sound: Update, J. Acoust. Soc. Am. 88 (1990) 2019–2021, https://doi.org/10.1121/1.400176.
[40] H.E. Bass, L.C. Sutherland, A.J. Zuckerwar, D.T. Blackstock, D.M. Hester, Atmospheric absorption of sound: Further developments, J. Acoust. Soc. Am. 97 (1995) 680–683, https://doi.org/10.1121/1.412989.
[41] E. Schäffer, S. Harkema, R. Blossey, U. Steiner, Temperature-gradient-induced instability in polymer films, Europhys. Lett. 60 (2002) 255–261, https://doi.org/10.1209/epl/i2002-00344-9.